

Catalytic Reduction of Graphene Oxide Nanosheets by Glutathione Peroxidase Mimetics Reveals a New Structural Motif in Graphene Oxide

Amit A. Vernekar and Govindasamy Mugesh*^[a]

Abstract: A catalytic reduction of graphene oxide (GO) by glutathione peroxidase (GPx) mimics is reported. This study reveals that GO contains peroxide functionalities, in addition to the epoxy, hydroxyl and carboxylic acid groups that have been identified earlier. It also is shown that GO acts as a peroxide substrate in the GPx-like catalytic activity of organoselenium/tellurium compounds. The reaction of tellurol, generated from the corresponding ditelluride, reduces GO through

the glutathione (GSH)-mediated cleavage of the peroxide linkage. The mechanism of GO reduction by the tellurol in the presence of GSH involves the formation of a tellurenic acid and tellurenyl sulfide intermediates. Interestingly, the GPx mimics also catalyze the

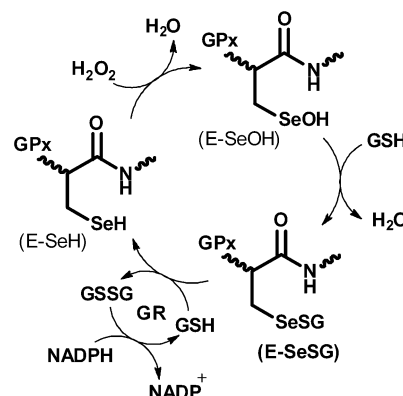
Keywords: decarboxylation • glutathione peroxidase • graphene • nanosheets • NMR spectroscopy • selenium

decarboxylation of the carboxylic acid functionality in GO at ambient conditions. Whereas the selenium/tellurium-mediated catalytic reduction/decarboxylation of GO may find applications in bioremediation processes, this study suggests that the modification of GO by biologically relevant compounds such as redox when using GO for biomedical applications because such modifications can alter the fundamental properties of GO.

Introduction

Glutathione peroxidase (GPx) is a well-known selenocysteine-containing mammalian enzyme that acts as an antioxidant and protects the cellular components from oxidative damage by catalytically reducing harmful peroxides in the presence of glutathione (GSH).^[1] During the catalytic cycle, the selenium moiety of the enzyme undergoes a series of oxidation and reduction reactions (Scheme 1). Initially, the selenol group reacts with H₂O₂ to produce the corresponding selenenic acid (E-SeOH), which further reacts with GSH to produce the selenenyl sulfide intermediate (E-SeSG). A nucleophilic attack of another GSH molecule at the sulfur center of the E-SeSG intermediate regenerates the active form of the enzyme (E-SeH) (Scheme 1).^[2] In the overall reaction, two equivalents of GSH are oxidized to glutathione disulfide (GSSG) and H₂O₂ is reduced to water.

During last three decades, several organoselenium compounds have been reported to mimic the activity of GPx.^[3] Although the selenium moieties in some of these compounds are quite different from that of GPx, these compounds efficiently catalyze the reduction of H₂O₂ and other related peroxides in the presence of GSH or aromatic thiols.^[3,4] In addition to organoselenium compounds, much



Scheme 1. Proposed catalytic mechanism of GPx, involving selenol, selenenyl sulfide, and selenenic acid intermediates. GR = glutathione reductase.

attention has been directed towards the design and synthesis of organotellurium compounds that mimic the action of GPx.^[5] Singh and co-workers reported that diaryl ditellurides are much more efficient catalysts than the selenium analogues in reducing H₂O₂ by using PhSH as a thiol co-substrate.^[6] Liu and co-workers showed that the GPx model, 2, 2'-ditellurobis(2-deoxy-β-cyclodextrin), exhibits high substrate specificity and remarkable catalytic efficiency when 3-carboxy-4-nitrobenzenethiol is used as a thiol substrate.^[7] Although several aliphatic and aromatic thiols have been used as co-substrates for the peroxidase-like reactions of selenium and tellurium compounds, the ability of these compounds to catalyze the reduction of substrates other than peroxides has not been studied. For the first time, we show

[a] A. A. Vernekar, Prof. Dr. G. Mugesh
Department of Inorganic and Physical Chemistry
Indian Institute of Science, Bangalore 560 012 (India)
Fax: (+91) 80 2360 1552
E-mail: mugesh@ipc.iisc.ernet.in

Supporting information for this article is available on the WWW under <http://dx.doi.org/10.1002/chem.201303339>.

that some of the GPx mimics exhibit new graphene oxide (GO) reductase and decarboxylase activities in the presence of GSH.

GO is a layered water-soluble material and a precursor for the bulk-scale production of graphene, which has captured a tremendous interest in various fields.^[8,9] Owing to its interesting properties and ease of processability, GO finds important use in polymers, ceramics, metal and thin-film electronics, hydrogen-storage composites, and carbocatalysis.^[10–16] GO has also been demonstrated as a chemotherapeutic delivery vehicle and to possess intrinsic peroxidase-like activity for highly selective and sensitive detection of glucose.^[17–19] Although these applications result from the remarkable properties of GO, the studies on new properties of GO appear to be challenging, which may widen its scope of applications. Whereas the Lerf–Klinowski model^[20] and the Dékány model^[21] suggest the probable structure of GO, the fundamental structure of GO is complex and still under debate. During our investigations on graphene-based nanomaterials,^[22] we found that GO can act as a peroxide substrate for GPx mimics. In the presence of GSH as a co-substrate, catalytic activity could be achieved. Interestingly, the diaryl ditelluride (**1**, Figure 2a), which has been shown to reduce hydroperoxides in the presence of thiols,^[6] effectively catalyzes the reduction of GO in the presence of GSH. Although this methodology yields good quality reduced graphene oxide (RGO) nanosheets at ambient temperature, the current investigation highlights a new property for both GO and GPx mimics and reveals the presence of peroxide linkages on GO (Figure 1). This would have a significant impact on its reactivity and behavior in broad range of applications of GO, which need to be rationalized from the view point of the proposed new structural motif.

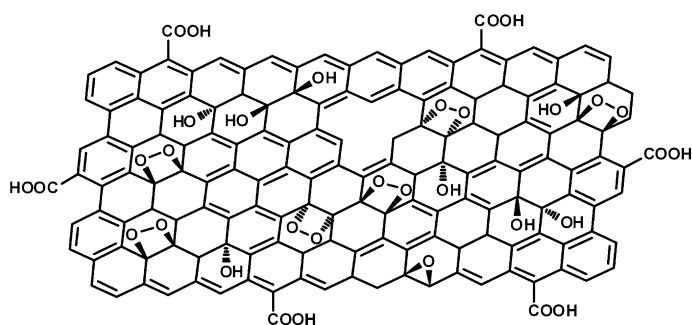


Figure 1. Proposed structure of GO containing peroxide linkages and epoxy-, hydroxyl-, and carboxylic acid groups.

Results and Discussion

Apart from the known, large sheet-like complex structures, the chemical functionalities on GO has been the topic of interest for quite some time. Among different models, the Lerf–Klinowski^[20] model, which is widely accepted, contributes to the understanding of the fundamental structure of

GO. According to this model, GO contains epoxy and hydroxyl as oxygen-containing functional groups. The revised version of the Lerf–Klinowski model further indicated the presence of carboxylic acid groups at the periphery of GO.^[23] Ajayan and co-workers revealed the presence of five- and six-membered-ring lactols as oxygenated functionalities on GO.^[24] However, the new reactivity and properties may originate from additional hidden functional groups on GO. Recent studies on the local structure of GO by Saxena et al. and others suggest that GO may contain peroxide linkages.^[25] The use of GO as catalyst for the oxidation reactions such as sulfoxidation,^[26] alkene oxidation,^[27a] alcohol oxidation,^[27a–b] amine oxidation,^[28] hydrocarbon oxidation,^[29] and so on, under mild conditions, suggests the presence of oxidizing functionalities such as peroxides. However, the spectroscopic techniques that are generally used to characterize GO are not sufficient to distinguish the peroxide linkages from epoxy groups. Therefore, chemical reactivity remains a reliable tool for chemists to probe the presence of peroxide groups.

Hummers method was employed to produce GO,^[30] which was ultrasonicated in water to yield a homogeneous dispersion of GO. Interestingly, in the preliminary test, GO responded positively for the peroxide starch/iodide reaction, giving rise to a violet-colored dispersion (Figure S1, the Supporting Information). We then envisaged that if peroxides form the integral part of GO, it may serve as a new substrate for GPx mimetics. Accordingly, when the GO dispersion was treated with small amount of **1** and GSH, a reduction of GO was observed at ambient temperature. In contrast, GSH alone was inefficient in reducing GO under identical conditions (Figure S2, the Supporting Information), indicating that the tellurium compound is responsible for the reduction in the presence of GSH. We further noticed that the ditelluride catalyst could be recovered and reused at least four times without a loss of its activity. The resulting product was thoroughly characterized to check the catalytic efficacy of the GPx mimetic (see below).

To understand whether the reduction of GO by compound **1** is similar to that of H₂O₂, we followed the reduction of GO by **1** by using a UV/Vis spectrometer. The decrease in absorbance of nicotinamide adenine dinucleotide phosphate (NADPH) was followed at 340 nm in the presence of glutathione reductase (GR) in phosphate buffer (pH 7.4) (Figure 2b and c). It is known that GR catalytically reduces GSSG to GSH by using NADPH as cofactor. In the control reactions, GSH or compound **1** alone in the absence of GSH did not show any reduction of GO (Figure 2c). These results suggest that GSH acts as cofactor in the catalytic cycle. The steady-state kinetics of the reduction process at different concentrations of GSH provided the Michaelis–Menten curve, indicating enzyme-like behavior (Figure 2d). From the plots of initial rate versus concentration of GSH and the Lineweaver–Burk plots (Figure 2e), it can be concluded that the reduction of GO by compound **1** follows an enzyme-like mechanism. The Michaelis constant (K_M) and maximum velocity (V_{max}) were found to be 7.3 mM and

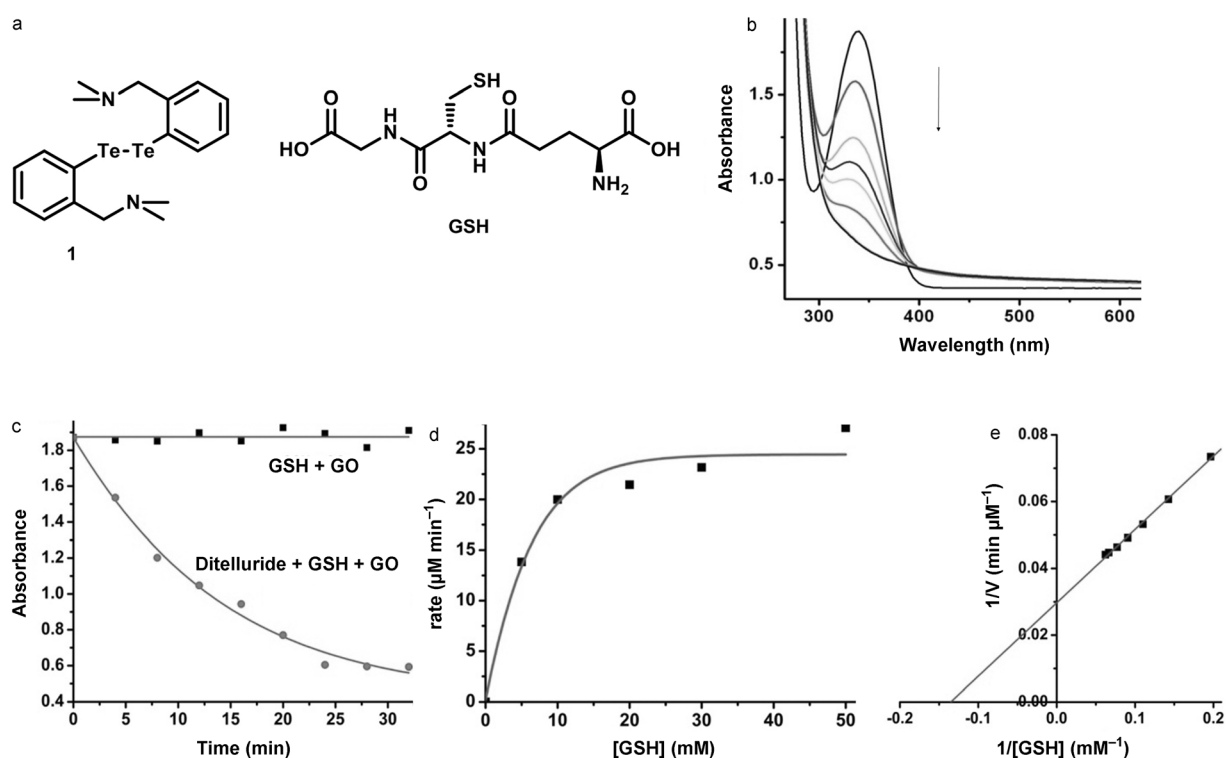


Figure 2. a) Structures of compound **1** and glutathione; b) UV/Vis spectra showing the decrease in the absorbance of NADPH during the progress of the reaction (different lines correspond to 4 min intervals); c) The exponential decrease of NADPH and the control reaction; d) The Michaelis–Menten curve; e) Lineweaver–Burk plot corresponding to Figure 1 d.

$33.9 \mu\text{M min}^{-1}$, respectively. Although a high value of K_M indicates a weak binding of GO to the tellurium center during the catalysis, it suggests that the release of reduced GO from the catalytic centre is favored.

We have also investigated the GO reductase activity of other GPx mimetics **2–7** (Figure 3a) and the natural GPx enzyme for a comparison. The initial reduction rates (Fig-

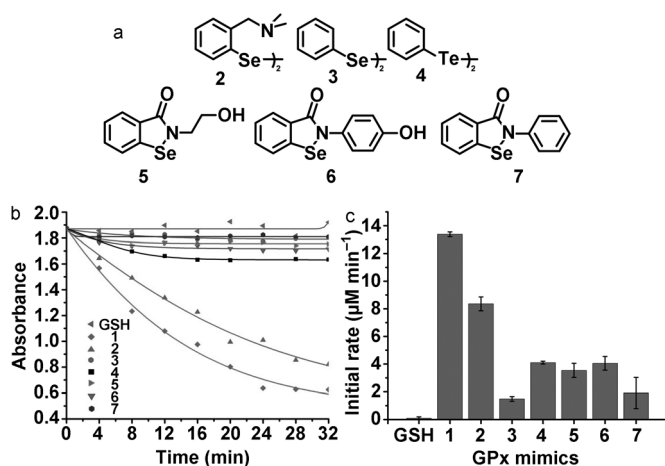


Figure 3. a) Structures of other GPx mimics; b) Relative GPx-like activities in the reduction of GO using GSH alone and compounds **1–7** in the presence of GSH; c) A comparison of the GO reductase activities of GPx mimics.

ure 3b and c) indicate that the activities of compound **1** and **2** are much higher compared with their GPx-like activity (H_2O_2 substrate). The higher catalytic activity of **1** and **2** can be attributed to the presence of tertiary amine group that acts as general base and facilitates the deprotonation of the tellurol/selenol produced by GSH-mediated reduction of the ditelluride/diselenide bond. In addition to the ditellurides (**1** and **4**) and diselenides (**2** and **3**), the cyclic compounds **5–7** also exhibited weak GO reductase activity. It should be noted that the Se–N covalent bond in ebselen (**7**) and related compounds is readily cleaved by thiols such as GSH, which is responsible for the GPx activity of these compounds.^[3] Similarly, the reaction of **1** and related ditellurides/diselenides with GSH produces the corresponding tellurols/selenols through the formation of tellurenyl sulfide/selenenyl sulfide intermediates.^[3,6] Although GPx contains a highly reactive selenocysteine residue, the enzyme was unable to reduce GO effectively. This is probably due to the fact that the large sheet-like structures of GO may not be accessible to the active site of GPx.

The formation of tellurenyl sulfide (**10**) was confirmed by ^{125}Te NMR spectroscopy. The peak observed at $\delta = 344$ ppm for compound **1** (Figure S3, the Supporting Information) disappeared after the addition of an excess of GSH with a new peak appearing at $\delta = 513$ ppm (Figure S4, Supporting Information) for the tellurenyl sulfide (**10**). The formation of **10** was also observed during the reduction of GO with **1** in the presence of GSH (Figure S5, the Supporting Information).

This probably indicates that the tellurol (**8**) rapidly reacts with peroxide functionalities on GO. It has been shown that thiols can open up the peroxide linkage in retinal pigment epithelial bisretinoids by attacking at the electrophilic carbon center.^[31] Considering the presence of peroxide functionalities on GO, the formation of tellurenic acid (**9**) was expected upon treatment of **8** with GO (Path A, Figure 4 a). However, our attempts to detect **9** by using ¹²⁵Te NMR spectroscopy were unsuccessful due to the facile reaction of GSH with **9**. The tellurol (**8**) is regenerated from **10** by reaction with GSH. Further attack of GSH at the sulfur center in the intermediate **11** results in the formation of a water molecule and glutathione disulfide (GSSG). Interestingly,

after 12 h of reaction time, a peak corresponding to **1** reappeared, probably due to aerial oxidation of the tellurol (**8**) (Figure S6, the Supporting Information).

To confirm that the tellurol (**8**) is actually responsible for the reduction of GO, we reduced compound **1** with NaBH₄ independently and then added to the mixture of GO and GSH. In this reaction, a very rapid reduction of GO was observed (see the video in the Supporting Information), which also confirms the presence of peroxide linkages on GO. In the absence of **1**, a mixture of NaBH₄ and GSH was unable to reduce GO under identical conditions. When the tellurol moiety in compound **8** was blocked by treatment with iodoacetic acid, no reduction of GO was observed. We further

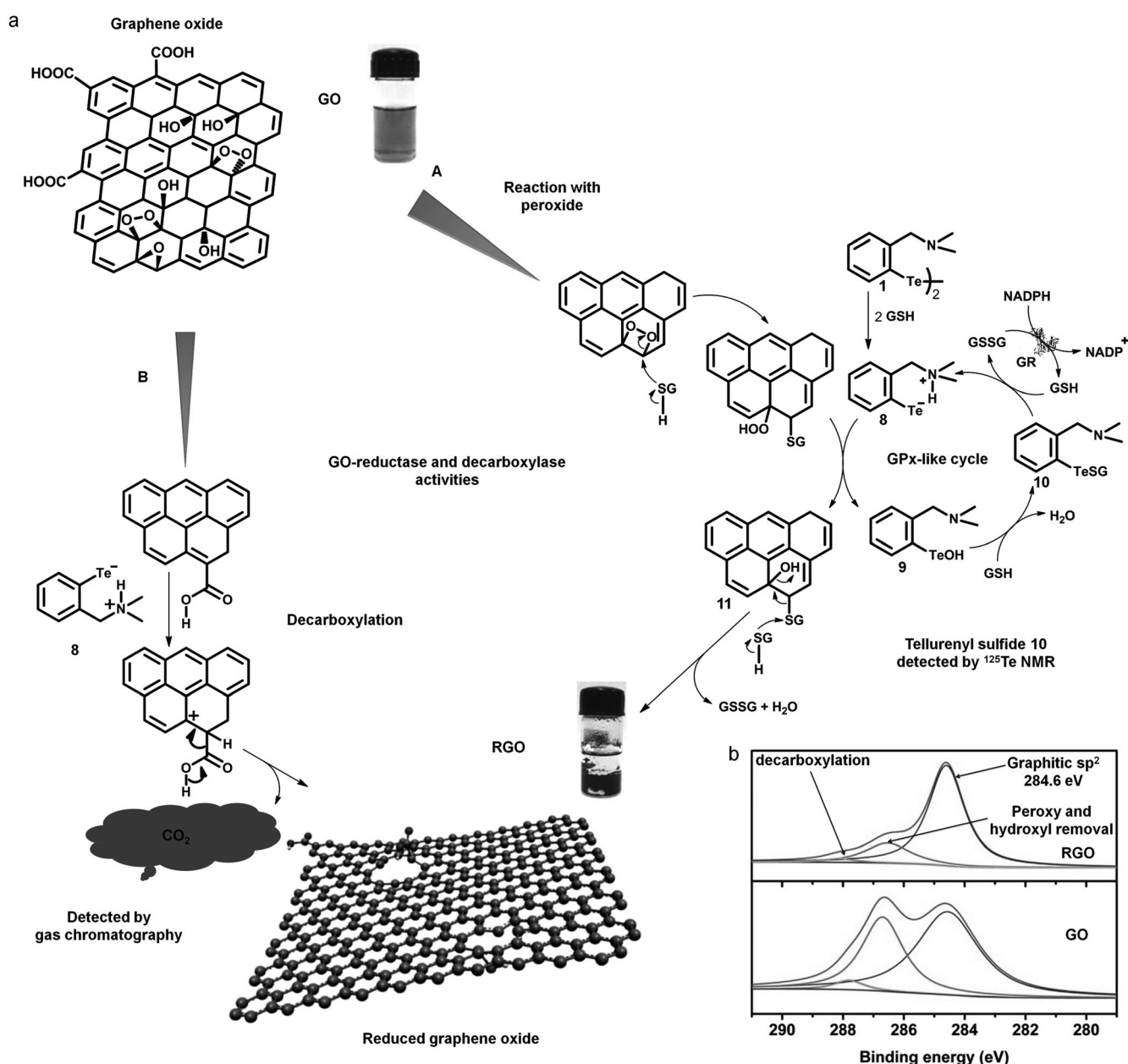


Figure 4. a) A detailed mechanism showing the different pathways (A and B) for the reduction of GO in the presence of compound **1** and GSH; b) Deconvoluted C1s X-ray photoelectron spectra (XPS) of GO and RGO. GR = glutathione reductase.

noticed a rapid evolution of a gas from the reaction mixture, which was confirmed as CO₂ by gas chromatographic analysis (Figure S7, the Supporting Information). The decrease in the carboxyl functionalities is also observed in the C1s X-ray photoelectron spectra (XPS) (Figure 4b) of the material obtained after reduction. These observations suggest that the GPx mimics not only reduce GO, but also act as an efficient decarboxylase to remove the carboxylate functionalities on GO at ambient temperature. The proposed mechanism for the decarboxylation is given in Figure 4a (Path B).

When a similar experiment was carried out using dithiothreitol (DTT) as a co-substrate instead of GSH, an immediate reduction of GO was observed. This is due to the stronger reducing ability of DTT that can effectively reduce the ditelluride bond in compound **1** to produce the tellurol (**8**). Extremely slow reactions were observed with DTT or GSH in the absence of **1**. In both the control reactions, no material separated out in the reaction vials even after 10 days, indicating that the reduction is ineffective. To understand whether compound **1** is regenerated during the catalytic cycle, we carried out the reduction of GO with a catalytic amount of **1** under a nitrogen atmosphere. However, a rapid reduction of GO was observed, indicating that the regeneration of compound **1** is not required for the catalytic activity. In addition to the demonstration of the new reactivity for the GPx mimics, this method can also be used to prepare RGO, which is a chemically generated form of graphene. It is well-known that graphene is a 2D and atomically thin sheet, which has interesting properties such as high mechanical strength, high surface area, high conductivity, and so on. Owing to the extraordinary properties, graphene finds remarkable applications in nanoelectronics, photonics, catalysis, biology, and so on.^[32–34] To confirm the formation of RGO under our experimental conditions, we further characterized this material thoroughly by using spectroscopic and microscopic methods and conductivity data.

The dispersion of GO changed its color gradually from brown to dark-brown and then finally to black within initial 30 min of reaction time (Figure S2, the Supporting Information). In the UV/Vis absorption spectra (Figure S8, the Supporting Information), GO exhibits the wavelength maxima at 230 nm due to $\pi-\pi^*$ transition originating from C=C. The broad band observed at 310 nm is attributed to the $n-\pi^*$ transition resulting from the C=O groups. The reduction of GO leads to a shift in the wavelength (to 265 nm), indicating a bathochromic shift, which is also associated with a hyperchromic effect. The FTIR spectra (Figure S9, the Supporting Information) also confirmed the formation of reduced graphene oxide (RGO). The signature frequencies due to the oxygen-containing functionalities such as carboxylic acid, hydroxyl and epoxide/peroxide groups in GO are significantly diminished upon reduction. This clearly indicates that the distorted conjugation in GO is restored in RGO after the reduction.

It is known that the oxidation of graphite by strong oxidizing reagents introduces a large amount of oxygen-containing functionalities as defects in GO, which exhibit D

band and broad G bands in the Raman spectra (Figure 5a). Pristine graphite exhibits a G band as the only characteristic feature of the first order scattering of the E_{2g} mode at 1570 cm⁻¹.^[35] Treatment of GO by using **1**-GSH mixture resulted in an increase in the intensity of I_D/I_G ratio to a lower extent compared with that of GO, indicating the restoration of the sp² conjugated network and formation of small aromatic domains. The I_D/I_G ratio (Table S1 in the Supporting Information) obtained from other methods are higher than that obtained from the reduction mediated by **1**-GSH (I_D/I_G=1.11). Recently, we reported that the GO reduced at higher temperature by a thiol-based reducing agent, dithiothreitol, shows an I_D/I_G ratio of about 1.06.^[22]

From the powder X-ray diffraction (XRD) patterns (Figure 5b), it is evident that the GO is exfoliated due to the introduction of oxygen-containing functional groups. Removal of these functional groups through reduction by **1**-GSH shifted the peak to $2\theta=24^\circ$, similar to the one observed for the pristine graphite with an increase in the d-spacing of 0.38 nm. This indicates the formation of exfoliated RGO. The reduction of GO was studied further with the help of X-ray photoelectron spectroscopy (XPS). The deconvoluted C1s XPS spectra of GO and RGO are given in Figure 4b. The appearance of strong peaks corresponding to the C–O and C=O groups reveals that the GO is highly oxygenated. On the other hand, the RGO produced after the reaction exhibits weaker peaks for C–O and C=O, indicating the effective reduction by **1**-GSH at the ambient temperature. The C/O ratio of the produced RGO was found to be 13.07. A comparison of the C/O ratios of RGO material obtained by various reduction methods is given in Table 1.

To illustrate the thermal stabilities of GO, RGO, and pristine graphite, thermogravimetric analysis (TGA) was carried out (Figure 5c). GO exhibits 11% decrease in weight due to the removal of intercalated and adsorbed water molecules between the layers of GO. At higher temperature (200 °C), a rapid decrease in the weight indicates the removal of oxygen-containing functional groups in GO. Interestingly, the TGA profile shows the higher thermal stability as the observed weight loss for RGO at 200 °C is only 4% under Ar gas flow. However, at a higher temperature (600 °C), the bulk pyrolysis of carbon skeleton is responsible for a further decrease in the weight, which is consistent with the TGA profile of GO and graphite. It should be mentioned that the reduction of GO with GSH alone at a higher temperature shows a weight loss of $\approx 10\%$ at 200 °C,^[44] which is significantly higher than that observed for the reduction by **1**-GSH.

Microscopic characterization of RGO by using SEM (Figure 5d) shows the randomly oriented exfoliated sheets of few microns. The TEM image (Figure 5e) indicates the formation of a silk-veil/wave-like structural morphology.^[35] Corrugation and scrolling, the intrinsic properties of graphene, are responsible for the observed wave-like structure of the RGO nanosheets. It has been shown that these two intrinsic properties render the thermodynamic stability to the nanosheets by bending.^[45] The AFM image (Figure 5f) with

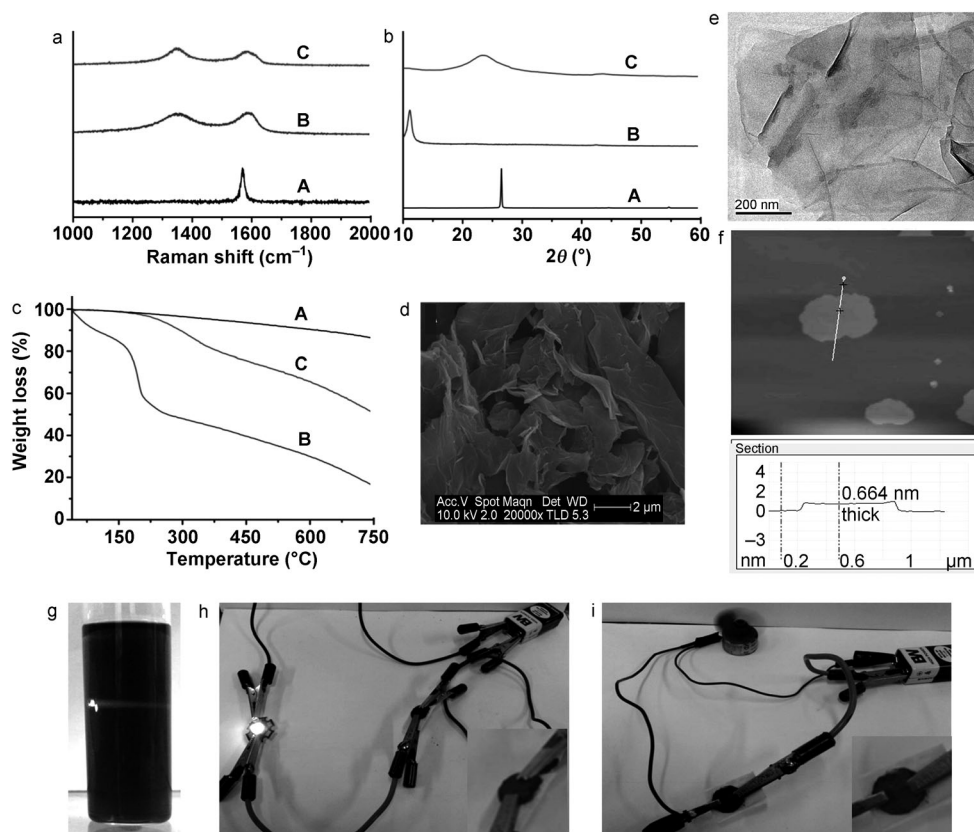


Figure 5. a) Raman spectra, b) X-ray diffraction (XRD) pattern, and c) thermogravimetry analysis (TGA) profile of pristine graphite (A), GO (B), and RGO (C); d) Scanning electron microscopy (SEM) image of RGO showing the crumpled nanosheets. e) Transmission electron microscopy (TEM) image showing RGO; f) Atomic force microscopy (AFM) image of RGO showing a single-sheet thickness of 0.664 nm; g) The stable dispersion of RGO in DMF showing the Tyndall effect upon irradiating with red laser light, indicating the colloidal stability owing to hydrophobicity; h), i) Experiments to confirm the conductivity of RGO (functioning of LED and motor when RGO is connected in a circuit); the inset of h and i show RGO pellets used for the experiments.

Table 1. Comparison of C/O ratios and electrical conductivities of graphene/RGO prepared by various methods.

Reducing agent/ methods	C/O ratio	Electrical conductivity [S m^{-1}]	Reference
NaBH_4	5.3	45	[36]
solvothermal	6.4	0.05	[37]
Na + EtOH			
N_2H_4	10.3	200	[38]
L-cysteine	increased	0.124	[39]
tea	–	53	[40]
aluminium powder	18.6	2100	[41]
Fe/HCl	7.9	2300	[42]
NaOH, solvothermal	–	3.6, 4.8, 267.8	[43]
and two-step reduction			
NaBH_4 , heating in H_2SO_4	4.78, > 8.57, > 246	82.3, 1660, 20200	[24]
and annealing at 1100°C			
ditelluride	13.07	544	present work

its height profile reveals the thickness of 0.664 nm. This thickness is consistent with the reported value for the single layer of graphene.^[46] The ^{13}C magic-angle spinning (MAS)-

NMR spectra of GO (Figure S10, the Supporting Information) shows the presence of a high amount of oxygenated carbon nuclei. The spectra show peaks at $\delta = 59.9$ and 68.6 ppm, which can be ascribed to the carbon atoms bearing peroxide and hydroxyl groups, respectively. The carbon that lacks oxygen functional groups exhibits a peak at $\delta = 130.3$ ppm, whereas the carbonyl carbon exhibits a peak at $\delta = 190.0$ ppm. The carbonyl carbon of the ester moiety also exhibits a small peak at $\delta = 166.9$ ppm, which is in agreement with an earlier report.^[24] On the other hand, due to the effective reduction of GO at room temperature by compound **1** in the presence of GSH, a broad peak was observed at $\delta \approx 106$ ppm. These observations suggest that the conjugation and formation of sp^2 domains are restored. The hydrophobic RGO was highly dispersible in DMF through which a Tyndall effect is observed upon irradiating with a red laser beam (Figure 5g).

The electrical conductivity of the RGO was found to be 544 S m^{-1} , indicating that the tellurol-mediated reduction is efficient in generating RGO with good conduc-

tivity. A comparison of the electrical conductivities of graphene prepared from different methods is represented in Table 1. The RGO produced by the present method was introduced into a small circuit to glow a battery operated 1 W light-emitting diode (LED) (Figure 5h) and a motor (Figure 5i). This suggests that the current methodology renders high quality RGO sheets by the reduction of oxygen-containing functionalities such as peroxide, hydroxyl, and carboxyl groups.

Conclusion

We show, for the first time, that graphene oxide (GO) can be reduced catalytically by glutathione peroxidase (GPx) mimetics. GO acts as a peroxide substrate in the GPx-like catalytic activity of organoselenium/tellurium compounds, indicating that GO contains peroxide functionalities. A detailed experimental investigation on a tellurium compound indicates that the synthetic tellurol reduces GO through cleavage of the peroxide ring. The mechanism of GO reduction by the tellurol in the presence of glutathione (GSH) involves the formation of a tellurenic acid and tellurenyl sulfide intermediates. In addition to the rapid cleavage of peroxide linkages, the GPx mimics also catalyze the decarboxylation of the carboxylic acid functionality in GO at ambient conditions. Although the catalytic reduction/decarboxylation of GO mediated by selenium/tellurium compounds may find applications in bioremediation processes, this study suggests that the modification of GO by biologically relevant compounds must be considered when using GO for biomedical applications.

Experimental Section

Characterization methods: Absorption spectra were acquired on Perkin-Elmer Lambda 750 UV/Vis spectrometer. Raman spectroscopy was performed on HORIBA JOBIN YVON LabRAM HR Raman spectrometer. IR spectra were obtained by using a Bruker IR spectrometer. X-ray photoelectron spectroscopy (XPS) was acquired on a MULTILAB 2000 THERMO SCIENTIFIC, UK. Thermogravimetric analysis (TGA) was carried out on a NETZSCH TG 209 F1 instrument at a heating rate of 2°C min⁻¹ from 40–750°C. Powder XRD pattern was recorded on PANalytical Xpert pro theta-two theta diffractometer by using a Cu_{Kα} (1.5406 Å) radiation. Scanning electron microscopy (SEM) images were recorded on Fei Sirion UHR SEM and ESEM Quanta. Atomic-force microscopy (AFM) images were acquired by using a Nanoscope V multi-mode atomic force microscope (Veeco Instruments, USA) operating in the tapping mode. Transmission electron microscopy (TEM) images and SAED pattern were recorded on TECNAI T20 transmission electron microscope operating at 200 KV after casting a drop of RGO dispersion in ethanol over Cu grid. Solid-state ¹³C MAS-NMR spectra were acquired on 300 MHz Bruker Avance solid-state NMR spectrometer using standard Bruker pulse programs.¹²⁵Te NMR spectra were obtained using 400 MHz Avance Bruker NMR spectrometer. The electrical conductivity of pellets prepared from the powder RGO sample was measured using the four point probe setup, Agilent Device Analyzer B1500 A with pulsed source 5 MHz.

GO reductase activity of compounds 1–7 in the presence of GSH: GSH (30 mg, 0.0976 mmol) was added to a 2 mL dispersion of GO

(2 mg mL⁻¹). An ethanolic solution of **1** (or **2–7**) was then added immediately to this mixture, such that the concentration of catalyst was 1 mM in the reaction mixture. This mixture was stirred, and at every 4 min interval, an aliquot from the reaction mixture (30 μL) was added to a quartz cuvette containing 0.4 mM NADPH and glutathione reductase (1.7 unit mL⁻¹) in phosphate buffer (100 mM, pH 7.4). The decrease in absorbance of NADPH at 340 nm was followed by using a UV/Vis spectrophotometer. The steady state kinetics experiments were carried out by using a similar method at different concentrations of GSH.

Quantitative production of RGO: GSH (40 mg, 0.130 mmol) was added to a GO dispersion (20 mL, 2 mg mL⁻¹). Diaryl ditelluride (**1**) (30 mg, 0.0573 mmol) dissolved in ethanol (2 mL) was then added to the above dispersion at ambient temperature. The reaction mixture was stirred for 2 h and then GSH (40 mg, 0.130 mmol) was added. After stirring for 12 h at room temperature, the mixture was centrifuged and washed with water and ethanol several times to obtain good quality RGO in quantitative yield.

Acknowledgements

This study was supported by the Department of Science and Technology (DST), New Delhi, India. G.M. acknowledges DST for the award of a Swarnajayanti Fellowship. The authors also acknowledge the Institute Nanoscience Initiative (INI) of Indian Institute of Science for providing the TEM facilities. A.A.V. thanks the Council of Scientific and Industrial Research (CSIR), New Delhi, India for a research fellowship.

- [1] a) L. Flohe, E. A. Günzler, H. H. Schock, *FEBS Lett.* **1973**, *32*, 132–134; b) J. T. Rotruck, A. L. Pope, H. E. Ganther, A. B. Swanson, D. G. Hafeman, W. G. Hoekstra, *Science* **1973**, *179*, 588–590.
- [2] a) O. Epp, R. Ladenstein, A. Wendel, *Eur. J. Biochem.* **1983**, *133*, 51–69; b) F. Ursini, M. Maiorino, R. Brigelius-Flohé, K.-D. Aumann, A. Roveri, D. Schomburg, L. Flohé, *Methods Enzymol.* **1995**, *252*, 38–53; c) C. Jacob, G. I. Giles, N. M. Giles, H. Sies, *Angew. Chem.* **2003**, *115*, 4890–4907; *Angew. Chem. Int. Ed.* **2003**, *42*, 4742–4758; d) G. Roy, B. K. Sarma, P. P. Phadnis, G. Magesh, *J. Chem. Sci.* **2005**, *117*, 287–303.
- [3] a) G. Magesh, H. B. Singh, *Chem. Soc. Rev.* **2000**, *29*, 347–357; b) G. Magesh, W.-W. du Mont, H. Sies, *Chem. Rev.* **2001**, *101*, 2125–2179; c) K. P. Bhabak, G. Magesh, *Acc. Chem. Res.* **2010**, *43*, 1408–1419; d) B. J. Bhuyan, G. Magesh, *Organoselenium Chemistry: Synthesis and Reactions* (Ed.: T. Wirth), Wiley-VCH, Weinheim, **2011**, pp. 361–392.
- [4] a) T. G. Back, B. P. Dyck, *J. Am. Chem. Soc.* **1997**, *119*, 2079–2083; b) T. G. Back, Z. Moussa, *J. Am. Chem. Soc.* **2002**, *124*, 12104–12105; c) S. S. Zade, H. B. Singh, R. J. Butcher, *Angew. Chem.* **2004**, *116*, 4613–4615; *Angew. Chem. Int. Ed.* **2004**, *43*, 4513–4515.
- [5] a) J. Malmström, M. Jonsson, I. A. Cotgreave, L. Hammarström, M. Sjödin, L. Engman, *J. Am. Chem. Soc.* **2001**, *123*, 3434–3440; b) L. Engman, D. Stern, I. A. Cotgreave, C.-M. Andersson, *J. Am. Chem. Soc.* **1992**, *114*, 9737; c) G. I. Giles, F. H. Fry, K. M. Tasker, A. L. Holme, C. Peers, K. N. Green, L.-O. Klotz, H. Sies, C. Jacob, *Org. Biomol. Chem.* **2003**, *1*, 4317–4322; d) C. W. Nogueira, G. Zeni, J. B. T. Rocha, *Chem. Rev.* **2004**, *104*, 6255–6285; e) A. L. Braga, E. E. Alberto, L. C. Soares, J. B. T. Rocha, J. H. Sudati, D. H. Roos, *Org. Biomol. Chem.* **2009**, *7*, 43–45; f) B. K. Sarma, D. Manna, M. Minoura, G. Magesh, *J. Am. Chem. Soc.* **2010**, *132*, 5364–5374.
- [6] G. Magesh, A. Panda, S. Kumar, S. D. Apte, H. B. Singh, R. J. Butcher, *Organometallics* **2002**, *21*, 884–892.
- [7] Z. Dong, J. Liu, S. Mao, X. Huang, B. Yang, X. Ren, G. Luo, J. Shen, *J. Am. Chem. Soc.* **2004**, *126*, 16395–16404.
- [8] a) D. Li, M. B. Muller, S. Gilje, R. B. Kaner, G. G. Wallace, *Nat. Nanotechnol.* **2008**, *3*, 101–105; b) V. C. Tung, M. J. Allen, Y. Yang, R. B. Kaner, *Nat. Nanotechnol.* **2009**, *4*, 25–29.
- [9] S. Park, R. S. Ruoff, *Nat. Nanotechnol.* **2009**, *4*, 217–223.

- [10] D. A. Dikin, S. Stankovich, E. J. Zimney, R. D. Piner, G. H. B. Dommett, G. Evmenenko, S. T. Nguyen, R. S. Ruoff, *Nature* **2007**, *448*, 457–460.
- [11] X. Qi, K. Pu, X. Zhou, H. Li, B. Liu, F. Boey, W. Huang, H. Zhang, *Small* **2010**, *6*, 663–669.
- [12] B. Kong, J. Geng, H. Jung, *Chem. Commun.* **2009**, 2174–2176.
- [13] R. Nouchi, K. Tanigaki, *Appl. Phys. Lett.* **2010**, *96*, 253503.
- [14] S. Watcharotone, D. Dikin, S. Stankovich, R. Piner, I. Jung, G. H. B. Dommett, G. Evmenenko, S. Wu, S. Chen, C. Liu, *Nano. Lett.* **2007**, *7*, 1888–1892.
- [15] C. Su, M. Acik, K. Takai, J. Lu, S. Hao, Y. Zheng, P. Wu, Q. Bao, T. Enoki, Y. Chabal, K. P. Loh, *Nat. Commun.* **2012**, *3*, 1298.
- [16] C. Su, K. P. Loh, *Acc. Chem. Rev.* **2013**, *46*, 2277–2285.
- [17] Z. Liu, J. T. Robinson, X. M. Sun, H. J. Dai, *J. Am. Chem. Soc.* **2008**, *130*, 10876–10877.
- [18] X. M. Sun, Z. Liu, K. Welsher, J. T. Robinson, A. Goodwin, S. Zaric, H. J. Dai, *Nano Res.* **2008**, *1*, 203–212.
- [19] Y. Song, K. Qu, C. Zhao, J. Ren, X. Qu, *Adv. Mater.* **2010**, *22*, 2206–2210.
- [20] a) A. Lerf, H. He, M. Forster, J. Klinowski, *J. Phys. Chem. B* **1998**, *102*, 4477–4482; b) D. Dreyer, S. Park, C. Bielawski, R. Ruoff, *Chem. Soc. Rev.* **2010**, *39*, 228–240.
- [21] T. Szabó, O. Berkesi, P. Forgó, K. Josepovits, Y. Sanakis, D. Petridis, I. Dékány, *Chem. Mater.* **2006**, *18*, 2740–2749.
- [22] A. A. Vernekar, G. Mugesh, *Chem. Eur. J.* **2012**, *18*, 15122–15132.
- [23] A. Rodríguez, P. Jimenez, *Carbon* **1986**, *24*, 163–167.
- [24] W. Gao, L. Alemany, L. Ci, P. Ajayan, *Nat. Chem.* **2009**, *1*, 403–408.
- [25] a) S. Saxena, T. Tyson, E. Negusse, *J. Phys. Chem. Lett.* **2010**, *1*, 3433–3437; b) S. Saxena, T. Tyson, S. Shukla, E. Negusse, H. Chen, J. Bai, *Appl. Phys. Lett.* **2011**, *99*, 013104; c) A. Eng, A. Ambrosi, C. Chua, F. Sanek, Z. Sofer, M. Pumera, *Chem. Eur. J.* **2013**, *19*, 12673–12683.
- [26] D. Dreyer, H. Jia, A. Todd, J. Geng, C. Bielawski, *Org. Biomol. Chem.* **2011**, *9*, 7292–7295.
- [27] a) D. R. Dreyer, H. P. Jia, C. W. Bielawski, *Angew. Chem.* **2010**, *122*, 6965–6968; *Angew. Chem. Int. Ed.* **2010**, *49*, 6813–6816; b) D. R. Dreyer, S. Murali, Y. Zh, R. S. Ruoff, C. W. Bielawski, *J. Mater. Chem.* **2011**, *21*, 3443–3447.
- [28] H. Huang, J. Huang, Y. Liu, H. He, Y. Cao, K. Fan, *Green Chem.* **2012**, *14*, 930–934.
- [29] H. Jia, D. Dreyer, C. Bielawski, *Tetrahedron* **2011**, *67*, 4431–4434.
- [30] W. Hummers, R. Offeman, *J. Am. Chem. Soc.* **1958**, *80*, 1339–1339.
- [31] K. Yoon, K. Yamamoto, J. Zhou, J. Sparrow, *Mol. Vision* **2011**, *17*, 1839–1849.
- [32] S. Stankovich, D. Dikin, G. Dommett, K. Kohlhaas, E. Zimney, E. Stach, R. Piner, S. Nguyen, R. Ruoff, *Nature* **2006**, *442*, 282–285.
- [33] F. Wang, Y. Zhang, H. Tian, C. Girit, A. Zettl, M. Crommie, Y. Shen, *Science* **2008**, *320*, 206–209.
- [34] S. Guo, S. Dong, *Chem. Soc. Rev.* **2011**, *40*, 2644–2672.
- [35] G. Wang, J. Yang, J. Park, X. Gou, W. Bang, H. Liu, J. Yao, *J. Phys. Chem. C* **2008**, *112*, 8192–8195.
- [36] H. J. Shin, K. K. Kim, A. Benayad, S. M. Yoon, H. K. Park, I. S. Jung, M. H. Jin, H. K. Jeong, J. M. Kim, J. Y. Choi, *Adv. Funct. Mater.* **2009**, *19*, 1987–1992.
- [37] M. Choucair, P. Thordarson, J. A. Stride, *Nat. Nanotechnol.* **2009**, *4*, 30–33.
- [38] S. Stankovich, D. Dikin, R. Piner, K. Kohlhaas, A. Kleinhammes, Y. Jia, Y. Wu, S. Nguyen, R. Ruoff, *Carbon* **2007**, *45*, 1558–1565.
- [39] D. Chen, L. Li, L. Guo, *Nanotechnology* **2011**, *22*, 325601.
- [40] V. Pham, T. Cuong, S. Hur, E. Oh, E. Kim, E. Shin, J. Chung, *J. Mater. Chem.* **2011**, *21*, 3371–3377.
- [41] Z. Fan, K. Wang, T. Wei, J. Yan, L. Song, B. Shao, *Carbon* **2010**, *48*, 1686–1689.
- [42] Z. Fan, W. Kai, J. Yan, T. Wei, Li. Zhi, J. Feng, Y. Ren, L. Song, F. Wei, *ACS Nano* **2011**, *5*, 191–198.
- [43] D. Luo, G. Zhang, J. Liu, X. Sun, *J. Phys. Chem. C* **2011**, *115*, 11327–11335.
- [44] T. Pham, J. Kim, J. Kim, Y. Jeong, *Colloids Surf. A* **2011**, *384*, 543–548.
- [45] G. Wang, X. Shen, B. Wang, J. Yao, J. Park, *Carbon* **2009**, *47*, 1359–1364.
- [46] J. I. Paredes, S. Villar-Rodil, P. Solís-Fernández, A. Martínez-Alonso, J. M. D. Tascón, *Langmuir* **2009**, *25*, 5957–5968.

Received: August 26, 2013
Published online: November 4, 2013